Resistive switching characteristics of maghemite nanoparticle assembly

2011 J. Phys. D: Appl. Phys. 44 085403

(http://iopscience.iop.org/0022-3727/44/8/085403)

IOP PUBLISHING JOURNAL OF PHYSICS D: APPLIED PHYSICS

J. Phys. D: Appl. Phys. **44** (2011) 085403 (6pp) doi:10.1088/0022-3727/44/8/085403

Resistive switching characteristics of maghemite nanoparticle assembly

Quanli Hu[1], Sung Mok Jung[2], Hyun Ho Lee[2], Yong-Sang Kim[1], Young Jin Choi[1], Dae-Hwan Kang[3], Ki-Bum Kim[4] and Tae-Sik Yoon[1]

[1] Department of Nano Science and Engineering, Myongji University, Yongin, Gyeonggi-do 449-728, Korea
[2] Department of Chemical Engineering, Myongji University, Yongin, Gyeonggi-do 449-728, Korea
[3] Memory Division, Semiconductor Business, Samsung Electronics Co. Ltd., Yongin, Gyeonggi-do 446-711, Korea
[4] Department of Materials Science and Engineering, Seoul National University, Seoul 151-742, Korea

E-mail: tsyoon@mju.ac.kr

Received 26 August 2010, in final form 22 November 2010
Published 8 February 2011
Online at stacks.iop.org/JPhysD/44/085403

Abstract

The resistive switching characteristics of the assembly of maghemite (γ-Fe_2O_3) nanoparticles having a diameter of ~10 nm were investigated in the structure of Al/γ-Fe_2O_3 nanoparticle multilayer (~300 nm thick)/Al-plate. The nanoparticle multilayer on Al plate was formed by repeating dip-coating processes. The multilevel (five states) resistive switching was observed with the resistance values ranging from $\sim 4.8 \times 10^5$ to 2.7×10^3 Ω depending on the externally applied voltage. The multilevel switching is thought to originate from the repetitive and reversible formation and rupture of multiple conducting filaments. It demonstrates the potential application of the γ-Fe_2O_3 nanoparticle assembly for resistive switching devices.

(Some figures in this article are in colour only in the electronic version)

1. Introduction

Resistive switching random access memory (ReRAM) with metal oxides has attracted increasing attention as a potential candidate for next generation nonvolatile memory device [1–14]. The ReRAM operates by the resistance change of metal oxides between the high-resistance state (HRS) and low-resistance state (LRS) by the externally applied electric field or current. Recent reports on the resistive switching phenomena in NiO, TiO_2, CuO, $SrTiO_3$, CoO, and others demonstrated the high-speed operation within tens of nanoseconds, the high HRS/LRS ratio with two or more orders of magnitude, excellent endurance and retention characteristics [3–11]. Various models have been proposed to explain the resistive switching, such as the formation and rupture of localized filamentary conducting path, reduced Schottky barrier height at the interface by the accumulation of charges or vacancies, etc [3–11]. In the filament model, the externally applied field or current reversibly forms and ruptures the localized filaments in metal oxides [4, 5, 7, 8]. As a result, their resistance is abruptly switched between HRS and LRS. Kwon *et al* directly observed the formation of localized filament composed of Ti_nO_{2n-1} by the electromigration of oxygen vacancies in Pt/TiO_2/Pt structure by high-resolution transmission electron microscopy analysis [11]. As another route for resistive switching, the oxygen vacancies or charges move through the oxides and accumulate at the interface with electrode by the applied field or current, and alter the Schottky barrier height at the interface [5]. It was also suggested that the movement of boundaries of the high-resistance region and the low-resistance region inside metal oxides in response to the external electric field causes the resistance change [12].

All the proposed mechanisms commonly adopt that the resistive switching is ascribed to the nanoscale redistribution of charges and defects, and change of phases inside metal oxides. In addition, the nanoscale resistive switching element will be employed in the ReRAM device as scaling down the device size. These motivate understanding of the resistive switching characteristics of nanomaterials such as nanowires and nanoparticles.

Until now, only a few studies have been reported on the resistive switching of nanowires and nanoparticles. Nagashima *et al* reported the multiscale bipolar resistive switching in cobalt oxide (Co_3O_4) nanowire with a size of

~10 nm [13]. The resistance of the nanowire was changed from HRS to LRS at positive voltage of $+V_{SET}$ (called the SET process), and then returns to HRS at a negative voltage of $-V_{RESET}$ (RESET), showing a bipolar switching. Lee *et al* also demonstrated the bipolar resistive switching from the Pt nanoparticle-embedded TiO_2 layer formed by layer-by-layer assembly [14]. The multilayer of TiO_2 layer and Pt nanoparticles were deposited by repeating the solution-based synthesis of the TiO_2 layer and attachment of negatively charged Pt nanoparticles. The resistive switching was achieved by trapping and detrapping the electrons in Pt nanoparticles. On the other hand, Kim *et al* observed another type of bipolar switching with magnetite (Fe_3O_4) nanoparticles assembly [15]. The Fe_3O_4 nanoparticle assembly undergoes HRS-to-LRS transition (SET) at $+V_{SET}$, and returns to HRS as the voltage decreases to 0 V (RESET). Then another SET transition occurs at $-V_{SET}$ and returns to HRS as the voltage decreases back to 0 V. They hypothesized that the resistive switching results from the movement of boundaries between conducting and insulating regions in the Fe_3O_4 nanoparticle assembly due to the responsive migration of Fe^{2+} and Fe^{3+} charges to the external field.

In this study, we investigated the resistive switching characteristics of the chemically synthesized colloidal maghemite (γ-Fe_2O_3) nanoparticle assembly in the structure of Al/γ-Fe_2O_3 nanoparticle multilayer/Al-plate. In particular, the use of colloidal nanoparticles has the advantage that the nanoparticle layer can be deposited by solution processes, which are cost-effective and also applicable to the organic and plastic substrates for flexible memory devices.

2. Experiment

The colloidal γ-Fe_2O_3 nanoparticles, stabilized by a surfactant of oleic acid ($C_{18}H_{34}O_2$), were synthesized through the decomposition of $Fe(CO)_5$ precursors following the method developed by Hyeon *et al* [16]. The oleic acid encapsulates the nanoparticle surface to prevent the aggregation in the solution, and the hydrophilic head of oleic acid is attached to the nanoparticle and the hydrophobic tail faces the solvent. Therefore, the nanoparticles have a hydrophobic character and are well dispersed in nonpolar solvent. The γ-Fe_2O_3 nanoparticles were dispersed in hexane with a concentration of $\sim 2.7 \times 10^{13}$ mL^{-1}, which was measured by an inductive coupled plasma atomic emission spectrometer (ICP-AES, Prodigy, Leeman Labs). The diameter of γ-Fe_2O_3 nanoparticles is ~10 nm as shown in figure 1, and the phase is maghemite (γ-Fe_2O_3, JCPDS No. 39-1346), which was confirmed by selected area electron diffraction pattern analysis in a transmission electron microscope (TEM, JEM2100F) [17, 18].

The γ-Fe_2O_3 nanoparticle multilayer was formed on an Al plate by repeating dip-coating processes. The Al plate was vertically dipped and pulled out with a speed of 0.1 mm s^{-1} and dried in air. During dip-coating, the nanoparticles adsorb on the surface of the Al plate and assemble as the solvent evaporates after pulling out the plate. Then, the dip-coated Al plate was annealed at 200 °C for 1 h in air to desorb the oleic acid molecules from the nanoparticle layer [18]. Because the oleic acids on the nanoparticle layer hinder the adsorption of nanoparticles at the subsequent dip-coating step [19], their desorption allows the formation of nanoparticle multilayer by repeating dip-coating. The desorption of oleic acid from the nanoparticle is also crucial to get the electrical properties because the organic surfactants (oleic acid) hinder the charge transport as an electrical insulator [15, 20]. The dip-coating and annealing steps were repeated ten times, so the γ-Fe_2O_3 nanoparticle multilayer was formed as shown in figure 2. Compared with the layer-by-layer assembly by the electrostatic force using glue layers [14, 21, 22], the adsorption of nanoparticles by, e.g., weaker van der Waals interaction facilitates the assembly of nanoparticles through their lateral migration upon the solvent evaporation. Also, because the electrically charged glue layers are not used, the assembly can be constructed only with nanoparticles, even with surfactants; therefore, it does not contain the remained charges in the assembly, which may affect the switching behaviour. The multilayer formation was analysed using the plan-view and oblique-angle view scanning electron microscope (SEM, JEM7401F) by folding and tilting the samples of γ-Fe_2O_3 nanoparticle multilayer on the Al plate.

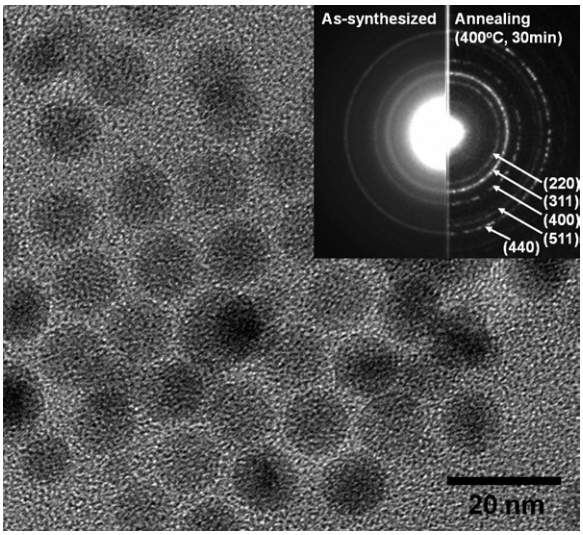

Figure 1. Plan-view TEM micrograph and electron diffraction pattern (inset) of γ-Fe_2O_3 nanoparticles.

For the electrical measurement, the patterned top Al electrode was deposited with a thickness of ~500 nm and a diameter of ~500 μm by sputtering with a hard mask on the γ-Fe_2O_3 nanoparticle multilayer/Al-plate. The post-metal annealing was carried out at 400 °C for 30 min in Ar environment. The γ-Fe_2O_3 nanoparticles did not transform to other phases after annealing, which was confirmed by selected area diffraction pattern analysis in TEM of nanoparticles on carbon-coated TEM grids (inset in figure 1). The current–voltage (I–V) curves of Al/γ-Fe_2O_3 nanoparticle multilayer/Al-plate were obtained using Agilent 4145B parameter analyser with a compliance current of 10 mA.

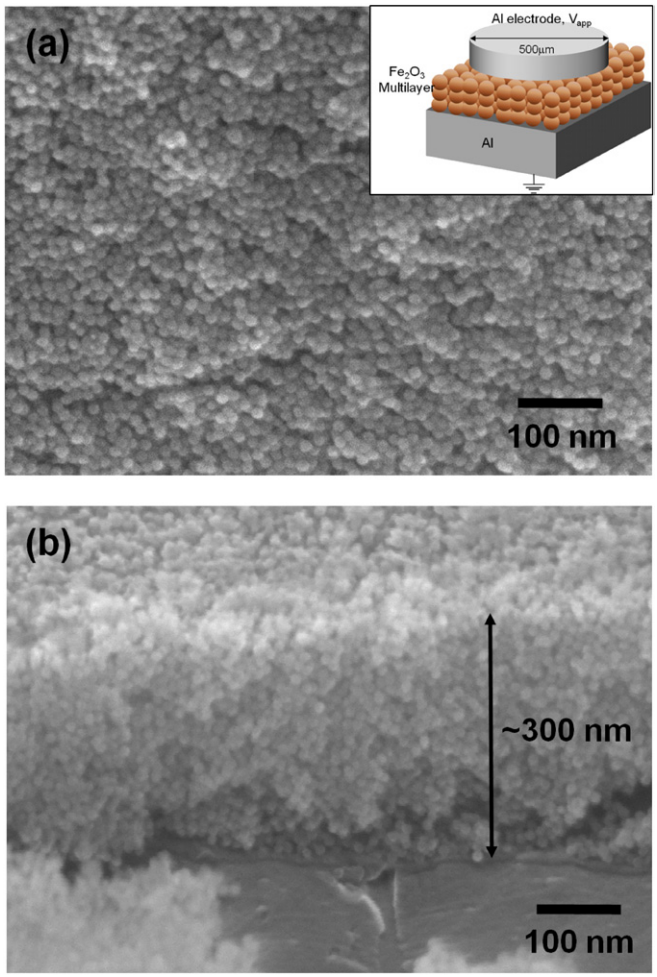

Figure 2. (*a*) Plan-view and (*b*) oblique-angle view SEM micrographs of γ-Fe_2O_3 nanoparticle multilayer on Al plate formed by repeating dip-coating and annealing steps ten times (inset: schematic of Al/γ-Fe_2O_3 nanoparticle multilayer/Al-plate structure).

3. Results and discussion

Figures 2(*a*) and (*b*) are the plan-view and oblique-angle view SEM micrographs of the γ-Fe_2O_3 nanoparticle multilayer on the Al plate formed by repeating dip-coating and annealing steps ten times. The inset is the schematic of the Al/γ-Fe_2O_3 nanoparticle multilayer/Al-plate structure. The thickness of the multilayer is measured to be ~300 nm. The multilayer could be formed without removing the surfactants if the nanoparticles were deposited by the convective assembly, during which the nanoparticles were driven on the nanoparticle layer by convective motion of nanoparticle as the solvent evaporates [23]. However, under the experimental condition of this study such as dip-coating speed, nanoparticle concentration and solvent evaporation rate, the adsorption of nanoparticles on the Al plate in the solution is a major route for the nanoparticle layer formation [19]. Thus, removing surfactants facilitates the multilayer formation.

Figure 3 is the *I*–*V* characteristics showing the multilevel resistive switching of Al/γ-Fe_2O_3 nanoparticle multilayer/Al-plate structure. Before obtaining the resistive switching, the initial soft breakdown process (forming) [4, 7, 8] by applying +7 V (flowing the compliance current of 1 mA) on the top Al electrode was carried out. The voltage on the top Al electrode was swept from 0 → +V → −V → 0 V. The resistance (=voltage/current) was measured at ±4 V. At the voltage sweeping range of ±6 V, the switching is not observed and the resistance at ±4 V is ~4.8×10^5 Ω (state I). The resistance was reduced to ~2×10^5 Ω (state II) when the voltage was swept from −8 → 0 V (figure 3(*a*)). State II was preserved at the voltage of ±10 V (figure 3(*b*)). While sweeping the voltage from 0 → +12 V, the resistance was further reduced to ~6.5×10^4 Ω (state III), and was preserved until the voltage was swept from +12 → −12 → 0 V (figure 3(*b*)). At ±14 V, LRS (state III)-to-HRS (state II) and HRS (state II)-to-LRS (state IV) transitions take place (figure 3(*c*)). The resistance of state IV is ~8.6×10^3 Ω. At ±16 V, the typical bipolar switching from LRS-to-HRS and HRS-to-LRS transition occurs (figure 3(*c*)). The lowest resistance state, state V, has a resistance of ~2.7×10^3 Ω. The current levels in the positive voltage regions of (*a*)–(*c*) are presented in figure 3(*d*), which clearly shows the five resistance states depending on the voltage range. States I to V have average resistance values of 4.8×10^5 Ω, 2×10^5 Ω, 6.5×10^4 Ω, 8.6×10^3 Ω and 2.7×10^3 Ω, respectively.

It is not conclusive which switching mechanism is predominant. However, the multilevel switching (five resistance states) between LRS and HRS with discrete resistance values implies that multiple conducting filaments were reversibly formed and ruptured. Odagawa *et al* reported the resistive switching in magnetite (Fe_3O_4) thin film, where the transition between Fe_3O_4 having low resistivity (~6.5 mΩ cm) and γ-Fe_2O_3 having high resistivity (>10^2 Ω cm) occurs at the interface by the redox process [24]. Although there is no definite evidence at the present data, the local phase transition of nanoparticle from γ-Fe_2O_3 to Fe_3O_4 and vice versa could be one of the possible routes for resistive switching. Because the resistance values are discrete from state I to V, it is rational that the multiple filaments were formed with different numbers at each state. Assuming that a single filament of the Fe_3O_4 phase is cylindrical with the same diameter as that of a nanoparticle (~10 nm), the number of filaments is calculated to be ~0.5, 1.2, 3.8, 29, and 92 at states I to V, respectively. Since the nanoparticle assembly has a close-packed structure (ABCABC stacking of the FCC structure), the cylindrical filament is not exactly normal to the surface. Also, the assembly has lots of structural defects, so the calculated values deviate from the integer numbers.

It should be discussed how the resistive switching associates the nanoscale redistribution of atoms or vacancies inside the γ-Fe_2O_3 nanoparticle assembly. The γ-Fe_2O_3 has an inverse spinel structure where oxygen anions construct the close-packed cubic cell and Fe^{3+} cations occupy the tetrahedral and octahedral sites with the presence of cation vacancies in octahedral sites [25]. With regard to the effect of distribution and state of cation vacancies in the spinel structure on the resistance, Lee *et al* observed the reduced resistance of magnetite (Fe_3O_4) nanoparticles and thin film by applying electric field at the temperature below the

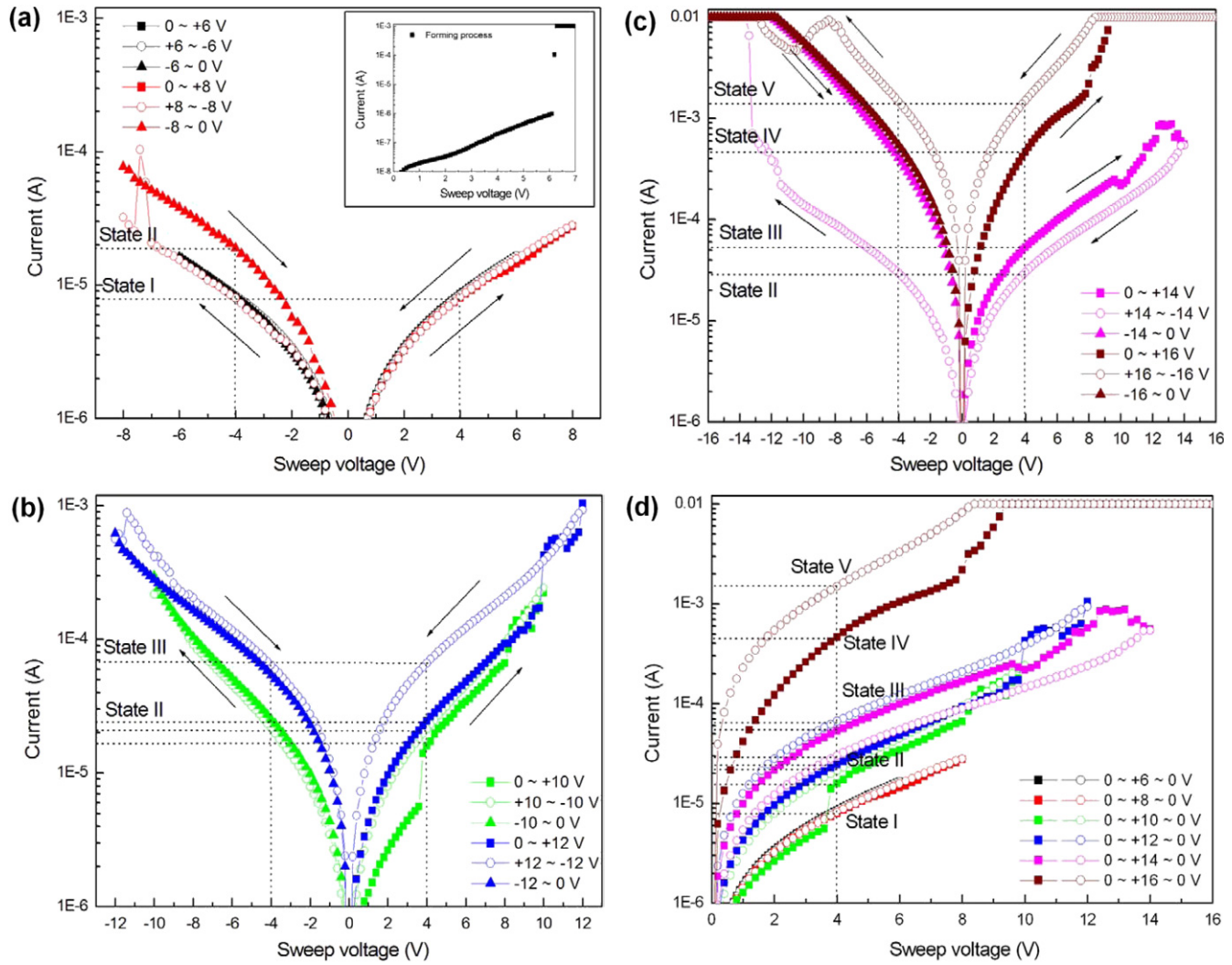

Figure 3. I–V characteristics of Al/γ-Fe_2O_3 nanoparticle multilayer/Al-plate structure at the different voltage sweep ranges; (*a*) ±6 and ±8 V, (*b*) ±10 and ±12 V, (*c*) ±14 and ±16 V and (*d*) summarized data of (*a*)–(*c*) in the positive voltage range.

Verwey temperature [20]. They explained that the resistance change is due to the breakdown of the insulating state when driven out of equilibrium state of distribution of atoms and vacancies by electrical field. Similarly, the local compositional change (atomic redistribution) should be accompanied for the phase transition of γ-Fe_2O_3 nanoparticles. In particular, the nanoparticle assembly has a large volume of interface between nanoparticles, where the atomic density is much lower than that inside the nanoparticles. These interfaces can afford to accept or donate the atoms and vacancies. As a result, they facilitate efficiently the redistribution of atoms and vacancies for the local phase transition of nanoparticles.

The high density of interface, considered as electrical defects, explains the electrical conduction mechanism by space charge limited current (SCLC) in the nanoparticle assembly. Figure 4(*a*) is the replot of the I–V curve in figure 3(*d*) in log–log scale. It shows the linear relation indicating that the electrical conduction follows either Ohmic or SCLC mechanism. The slope of $\log(I)$–$\log(V)$ curve is presented in figure 4(*b*). Irrespective of the resistance states (states I to V), $\mathrm{d}\log(I)/\mathrm{d}\log(V)$ values are close to unity ($<\sim$1.5) at small voltage range ($<\sim$4 V), demonstrating the Ohmic conduction ($I \propto V$). With increasing voltage, the $\mathrm{d}\log(I)/\mathrm{d}\log(V)$ values increase. Although the values are statistically scattered, most data points are close to $\sim$2 at the voltage $<\sim$8 V, implying the SCLC conduction mechanism ($I \propto V^2$) [26]. The $\mathrm{d}\log(I)/\mathrm{d}\log(V)$ values are further scattered at the voltage $>\sim$8 V, where the resistance changes mostly occur. The conduction behaviour of resistive switching metal oxide showing the Ohmic conduction at the low voltage and transition to SCLC at higher voltage was previously reported [27, 28]. At the low voltage, the injected current density is lower than the thermally generated carrier density, so the Ohmic conduction is dominant. With increasing voltage, the injected current is higher; therefore SCLC would predominate while filing the trap sites [27]. The I–V curve could not be fitted to other conduction mechanisms such as Schottky emission, tunnelling and Poole–Frenkel conduction, so they were ruled out. Because the nanoparticle assembly has a large volume of interface that acts as trap sites, the current would flow through the filaments by the SCLC conduction as filling nearby trap sites.

As with the thin film of metal oxide [5], the resistive switching of the nanoparticle assembly has the issue of

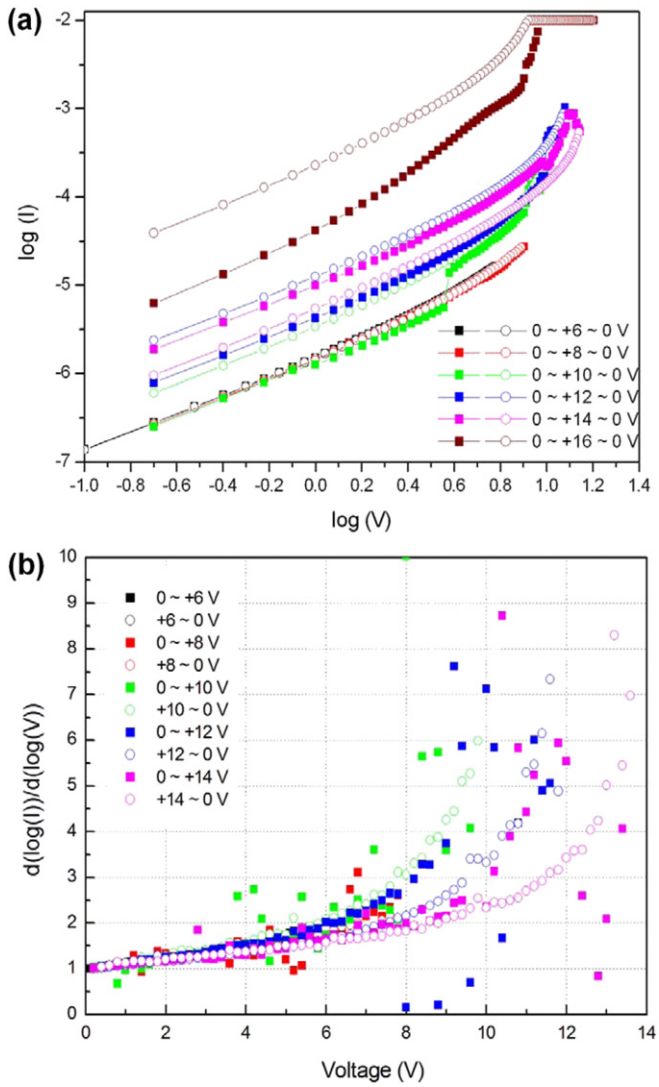

Figure 4. (*a*) Replot of I–V curve in log–log scale and (*b*) slope of log(I)–log(V) curve in the positive voltage range.

characteristic variation. Applying a high voltage or current does not always form the filament, but also rupture it at the same time, because both the formation and rupture of filaments are caused by the locally concentrated electrical field or current. The random formation and rupture of filaments would limit to obtain the uniform and reproducible switching characteristics for practical applications. In particular, a large volume of interface in the nanoparticle assembly may cause rather irregular switching than in the thin film structure. But the increased interface volume is inevitable even in the thin film structure as scaling down the device size. Therefore, it will be required to control the resistive switching in a single or a few nanoparticles or nanowires for highly scaled devices. In this study, the diameter of the Al top electrode is $\sim$500 μm, so the resistive switching actually comes out from the switching of a large number of nanoparticles. It is worth further investigating the dependence of multilevel switching and its uniformity on the thickness and lateral size of the nanoparticle assembly in the nanopatterned structure.

4. Conclusion

We demonstrated the multilevel resistive switching in the structure of the Al/γ-Fe_2O_3 nanoparticle multilayer ($\sim$300 nm thick)/Al-plate. The five resistant states with magnitudes of $\sim 4.8 \times 10^5$, 2×10^5, 6.5×10^4, 8.6×10^3 and 2.7×10^3 Ω were achieved depending on the voltage. The multilevel switching is thought to result from the formation and rupture of multiple conducting filaments by the external voltage. The electrical conduction in the nanoparticle assembly follows Ohmic conduction at low voltage and SCLC conduction as the voltage increases owing to the presence of interface traps between nanoparticles. Although a further study is required, the facilitated formation and rupture of multiple filaments in the γ-Fe_2O_3 nanoparticle assembly provides the feasibility for the application to multilevel resistive switching elements.

Acknowledgment

This work was supported by the 2010 research fund of Myongji University in Korea.

References

[1] Hiatt W R and Hickmott T W 1965 Bistable switching in niobium oxide diode *Appl. Phys. Lett.* **6** 106–8
[2] Bruyere J C and Chakraverty B K 1970 Switching and negative resistance in thin films of bickel oxide *Appl. Phys. Lett.* **16** 40–3
[3] Beck A, Bednorz J G, Gerber C, Rossel C and Widmer D 2000 Reproducible switching effect in thin oxide films for memory application *Appl. Phys. Lett.* **77** 139–41
[4] Choi B J, Jeong D S, Kim S K, Rohde C, Choi S, Oh J H, Kim H J, Hwang C S, Szot K, Waser R, Reichenberg B and Tiedke S 2005 Resistive switching mechanism of TiO_2 thin films grown by atomic-layer deposition *J. Appl. Phys.* **98** 033715
[5] Sawa A 2008 Resistive switching in transition metal oxides *Mater. Today* **11** 28–36
[6] Rozenberg M J, Inoue I H and Sanchez M J 2004 Nonvolatile memory with multilevel switching: a basic model *Phys. Rev. Lett.* **92** 178302
[7] Kim D C *et al* 2006 Electrical observations of filamentary conductions for the resistive memory switching in NiO films *Appl. Phys. Lett.* **88** 202102
[8] Yoshida C, Tsunoda K, Noshiro H and Sugiyama Y 2007 High speed resistive switching in Pt/TiO_2/TiN film for nonvolatile memory application *Appl. Phys. Lett.* **91** 223510
[9] Kim S and Choi Y K 2009 A comprehensive study of the resistive switching mechanism in Al/TiO_x/TiO_2/Al-structured RRAM *IEEE Trans. Electron Devices* **56** 3049–54
[10] Choi H, Jung H, Lee J, Yoon J, Park J, Seong D J, Lee W, Hasan M, Jung G Y and Hwang H 2009 An electrically modifiable synapse array of resistive switching memory *Nanotechnology* **20** 345201
[11] Kwon D H, Kim K M, Jang J H, Jeon J M, Lee M H, Kim G H, Li X S, Park G S, Lee B, Han S, Kim M and Hwang C S 2010 Atomic structure of conducting nanofilaments in TiO_2 resistive switching memory *Nature Nanotechnol.* **5** 148–53
[12] Strukov D B, Snider G S, Stewart D R and Williams R S 2008 The missing memristor found *Nature* **453** 80–3
[13] Nagashima K, Yanagida T, Oka K, Taniguchi M, Kawai T, Km J S and Park B H 2010 Resistive switching multistate

nonvolatile memory effects in a single cobalt oxide nanowire *Nano Lett.* **10** 1359–63
[14] Lee C, Kim I, Shin H, Kim S and Cho J 2010 Nonvolatile memory properties of Pt nanoparticle-embedded TiO_2 nanocomposite multilayers via electrostatic layer-by-layer assembly *Nanotechnology* **21** 185704
[15] Kim T H, Jang E Y, Lee N J, Choi D J, Lee K J, Jang J T, Choi J S, Moon S H and Cheon J 2009 Nanoparticle assemblies as memristors *Nano Lett.* **9** 2229–33
[16] Hyeon T, Lee S S, Park J, Chung Y and Na H B 2001 Synthesis of highly crystalline and monodisperse maghemite nanocrystallites without a size-selection process *J. Am. Chem. Soc.* **123** 12798–801
[17] Seo I, Kwon C W, Lee H H, Kim Y S, Kim K B and Yoon T S 2009 Assembly of colloidal nanoparticles into anodic aluminum oxide templates by dip-coating process *IEEE Trans. Nanotechnol.* **8** 707–12
[18] Seo I, Kwon C W, Lee H H, Kim Y S, Kim K B and Yoon T S 2009 Completely filling anodic aluminum oxide with maghemite nanoparticles by dip coating and their magnetic properties *Electrochem. Solid-State Lett.* **12** K59–K62
[19] Yoon T S, Oh J, Park S H, Kim V, Jung B G, Min S H, Park J, Hyeon T and Kim K B 2004 Single and multiple-step dip-coating of colloidal maghemite (γ-Fe_2O_3) nanoparticles onto Si, Si_3N_4, and SiO_2 substrates *Adv. Funct. Mater.* **14** 1062–8
[20] Lee S, Fursina A, Mayo J T, Yavuz C T, Colvin V L, Sofin R G S, Shvets I V and Natelson D 2008 Electrically driven phase transition in magnetite nanostructures *Nature Mater.* **7** 130–3
[21] Kotov N A, Dékány I and Fendler J H 1995 Layer-by-layer self-assembly of polyelectrolyte-semiconductor nanoparticle composite films *J. Phys. Chem.* **99** 13065–9
[22] Sun S, Anders S, Hamann H F, Thiele J U, Baglin J E E, Thomson T, Fullerton E, Murray C B and Terris B D 2002 Polymer mediated self-assembly of magnetite nanoparticles *J. Am. Chem. Soc.* **124** 2884–5
[23] Dimitrov A S and Nagayama K 1996 Continuous convective assembling of fine particles into two-dimensional arrays on solid surfaces *Langmuir* **12** 1303–11
[24] Odagawa A, Katoh Y, Kanzawa Y, Wei Z, Mikawa T, Muraoka S and Takagi T 2007 Electroforming and resistance-switching mechanism in a magnetite thin film *Appl. Phys. Lett.* **91** 133503
[25] Bastow T J, Trinchi A, Hill M R, Harris R and Muster T H 2009 Vacancy ordering in γ-Fe_2O_3 nanocrystals observed by ^{57}FeNMR *J. Magn. Magn. Mater.* **321** 2677–81
[26] Rose A 1955 Space-charge-limited currents in solids *Phys. Rev.* **97** 1538–44
[27] Kim K M, Choi B J, Shin Y C, Choi S and Hwang C S 2007 Anode-interface localized filamentary mechanism in resistive switching of TiO_2 thin films *Appl. Phys. Lett.* **91** 012907
[28] Xia Y, He W, Chen L, Meng X and Liu Z 2007 Field-induced resistive switching based on space-charge-limited current *Appl. Phys. Lett.* **90** 022907